PROTEINS: Structure, Function, and Genetics 32:362–380 (1998)

Engineering an Mg^{2+} Site to Replace a Structurally Conserved Arginine in the Catalytic Center of Histidyl-tRNA Synthetase by Computer Experiments

John G. Arnez, Karen Flanagan, Dino Moras, and Thomas Simonson*
Laboratoire de Biologie Structurale, Institut de Génétique et de Biologie Moléculaire et Cellulaire (Centre National de la Recherche Scientifique/Institut National de la Santé et de la Recherche Médicale/Université Louis Pasteur), Strasbourg-Illkirch, France

ABSTRACT **Histidyl-tRNA synthetase (HisRS) differs from other class II aminoacyl-tRNA synthetases (aaRS) in that it harbors an arginine at a position where the others bind a catalytic Mg^{2+} ion. In computer experiments, four mutants of HisRS from *Escherichia coli* were engineered by removing the arginine and introducing a Mg^{2+} ion and residues from seryl-tRNA synthetase (SerRS) that are involved in Mg^{2+} binding. The mutants recreate an active site carboxylate pair conserved in other class II aaRSs, in two possible orders: Glu-Asp or Asp-Glu, replacing Glu-Thr in native HisRS. The mutants were simulated by molecular dynamics in complex with histidyl-adenylate. As controls, the native HisRS was simulated in complexes with histidine, histidyl-adenylate, and histidinol. The native structures sampled were in good agreement with experimental structures and biochemical data. The two mutants with the Glu-Asp sequence showed significant differences in active site structure and Mg^{2+} coordination from SerRS. The others were more similar to SerRS, and one of them was analyzed further through simulations in complex with histidine, and His+ATP. The latter complex sampled two Mg^{2+} positions, depending on the conformation of a loop anchoring the second carboxylate. The lowest energy conformation led to an active site geometry very similar to SerRS, with the principal Mg^{2+} bridging the α- and β-phosphates, the first carboxylate (Asp) coordinating the ion through a water molecule, and the second (Glu) coordinating it directly. This mutant is expected to be catalytically active and suggests a basis for the previously unexplained conservation of the active site Asp-Glu pair in class II aaRSs other than HisRS. Proteins 32:362–380, 1998.**

Key words: molecular dynamics simulations; mutagenesis; aminoacyl-tRNA synthetase; ATP

INTRODUCTION

Aminoacylation of a tRNA by its cognate amino acid is a two-step reaction. The first step is the formation of a mixed anhydride, the aminoacyl-adenylate, from adenosine triphosphate (ATP) and amino acid, with release of pyrophosphate. The second step is the transfer of the aminoacyl moiety to the 2' or 3' OH of the terminal ribose of the tRNA, with release of adenosine monophosphate (AMP). The entire reaction is catalyzed by a family of enzymes, the aminoacyl-tRNA synthetases (aaRS). Each aaRS is specific for one amino acid and a set of cognate tRNAs, known as isoacceptors. The aaRS family can be divided into two classes based on homologous sequence and structural motifs,[1] which lead to two different architectures of the active site.[2,3] Here, we focus on interactions that occur during the first step of the overall reaction in histidyl-tRNA synthetase, *i.e.*,, the formation of histidyl-adenylate.

Histidyl-tRNA synthetase (HisRS) is a homodimeric class II aaRS. The monomer consists of two structural domains.[4] The C-terminal domain is an α-β structure implicated in binding the anticodon of $tRNA^{His}$. The N-terminal domain contains the active site, formed of a seven-stranded antiparallel β-sheet surrounded by α-helices and containing the three class II signature motifs. The active site is a platform that binds histidine and ATP and fixes them in the correct mutual orientation[4,5] (Fig. 1a). The floor of the histidine-binding pocket is formed by a glycine-rich portion of the β-sheet, and the sides are formed by the HisRS-conserved motifs HisA (*Escherichia coli* residues 257–264) and HisB (residues 284–292) and the conserved Glu131, which is at the carboxy end of motif 2. The ATP moiety is held in place by class II conserved residues, most notable of which are the motif 2 arginine 113, the motif 2 loop arginine 121, and the motif 3 arginine 311. The last two interact with the γ-phosphate of the ATP, whereas

*Correspondence to: Thomas Simonson, Institut de Génétique et de Biologie Moléculaire et Cellulaire, BP 163, 67404 Strasbourg-Illkirch, France. E-mail: simonson@igbmc.ustrasbg.fr
Received 27 January 1998; Accepted 26 March 1998

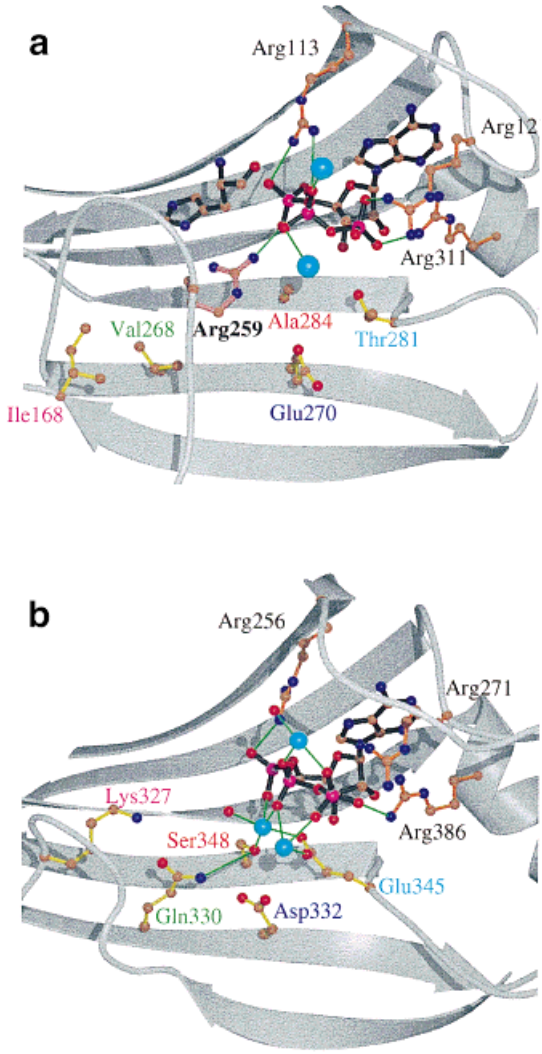

Fig. 1. Ribbon diagram of the active site of (**a**) HisRS[5] and (**b**) SerRS[6], complexed with ATP. The HisRS site also contains an analog of histidine, histidinol. Shown are the two class II conserved arginines (a, Arg 113 and Arg 311; b, Arg 256 and Arg 386) and the nearly invariant arginine (a, Arg 121; b, Arg 271). The metal ions are shown in light blue; there are two in HisRS (a) and three in SerRS (b). Arg 259 in (a) takes the place of the metal ion bridging the **α**- and **β**-phosphates in (b); it is replaced by Gly in the mutants studied here. Also shown are the residues in HisRS (a) that are replaced by similarly positioned residues in SerRS (b). This and the other structure figures were generated with the programs MOLSCRIPT[43] and RASTER3D[44,45].

Arg113 interacts with the α-phosphate. In addition to these arginines, HisRS is unique among class II aaRSs in that it possesses a fourth arginine, Arg259, which is part of the conserved HisA motif (Fig. 1a). This arginine interacts with the α-phosphate; its guanidino group replaces a metal ion found in SerRS[5] and thought to exist in all other class II aaRSs. Three metal sites were observed in SerRS by anomalous dispersion of Mn^{2+} ions and are presumed to correspond to actual Mg^{2+} sites.[6] Arg259 replaces the principal site, *i.e.,* the one with the highest occupancy, which interacts with the α-phosphate. The other two bridge the β- and γ-phosphates (Fig. 1b) and were recently observed in HisRS as well.[5]

In addition to their role in binding ATP, these ions, particularly the principal ion when present, are presumed to play a role in aaRS catalysis by stabilizing the pentavalent and highly charged α-phosphate in the transition state. A catalytic role for Mg^{2+} ions in the exonuclease mechanism of DNA polymerase I has been suggested and supported by mutagenesis experiments as well as detailed simulations.[7,8] In HisRS, the Mg^{2+} proxy Arg259 was shown to contribute to catalysis by mutation experiments that removed this side chain. For example, the R259H mutation slows the adenylation reaction by three orders of magnitude.[5]

The HisRS active site is unusual in yet another aspect. Most class II aaRSs, such as AspRS[9,10] and SerRS,[6] have two conserved carboxylates adjacent to the β-strand of motif 3. The first carboxylate, an Asp, extends from the β-strand distal to the motif 3 strand. The second carboxylate, a Glu, is on a loop preceding the β-strand proximal to the motif 3 strand (Fig. 1b). This Glu coordinates the principal metal ion directly, whereas the Asp interacts with the ion via a water molecule. In HisRS, the first carboxylate is Glu270, but the second carboxylate is replaced by a threonine, Thr281 (Fig. 1a). The most obvious role of Glu270 in HisRS appears to be positioning Arg259.[5] The present study suggests that the identity of the more common Asp-Glu pair is important for correct positioning of the principal metal ion.

Another feature of the HisRS active site that is shared by all class II aaRSs, but is unique with respect to all other ATP- or GTP-binding proteins, is the completely bent geometry of the bound ATP. A highly bent geometry is also observed in three ATP structures in the Cambridge Structural Database in the presence of sodium counterions (entries adentp[11] and citwux10[12]). Two ATP structures in the presence of divalent Mg^{2+} or Mn^{2+} ions are found in the data base (entries cicrah10[13] and decdiy[14]), in which the ATP is less bent and coordinates the ion with all three phosphates. The ATP environment in the protein is very different. The analysis of a mutant HisRS:His:ATP complex below is expected to provide insights into this protein-ATP interaction mode.

To understand these unique features of HisRS, we have examined through computer simulations the possibility of engineering an Mg^{2+} site into HisRS that would functionally replace Arg259. This exercise is of general interest, since the engineering of metal-binding sites in enzymes makes it possible to fine-tune catalysis and has potential applications in industry and medicine. Ab initio engineering of metal-binding sites is a difficult task, for it requires concerted changes not only at the site of metal binding but also in other parts of the target mol-

ecule.[15–18] In this study, we are not designing a site ab initio, but transferring a site from a similar framework, already optimized through evolution. Related engineering exercises have been carried out experimentally: a manganese-binding site was transplanted from manganese peroxidase into cytochrome c oxidase by mutagenesis,[19] and a magnesium-binding site was transplanted from oncomodulin into parvalbumin.[20] Comparing the *E. coli* HisRS active site with that of SerRS, we construct a series of targeted mutations of some critical residues in HisRS. The simulations then address the question of whether the modified HisRS has an active site that is stable and likely to be catalytically active. We first remove the side chain of Arg259 by mutating it to a Gly. Arg259 is in a loop that is shorter in SerRS, but we retain the length of the HisRS loop so that the remaining residues of the conserved HisA motif will not be perturbed. Next, we replace the guanidino group of the arginine with an Mg^{2+} site, by transplanting four combinations of some key residues from SerRS into HisRS. The resulting mutated proteins, complexed with histidyl-adenylate (HisAMP), are subjected to molecular dynamics simulation. The metal sites thus constituted are compared with the strongest Mn^{2+} site in the SerRS active site. The most promising mutant, *i.e.*, the one that most closely recapitulates the strongest site in SerRS, undergoes further molecular dynamics simulations, in complex with histidine, and with histidine and ATP. The resulting structures present a metal coordination similar to SerRS and are expected to be catalytically active.

Simulations of the native HisRS were carried out as controls, in complexes with His, HisAMP, and the inhibitor histidinol (HisOH). Experimental structures are known for native *E. coli* HisRS complexed with HisOH and ATP, and with HisAMP. The HisAMP simulations can be compared directly with the latter structure. In addition, the structure of HisRS from *Thermus thermophilus* complexed with His[21] became available in the final stage of this work. The simulations with His and HisOH can be compared with both the latter experimental structure and the HisOH+ATP complex, providing insights into the ordering of the active site prior to ATP binding.

MATERIALS AND METHODS

The simulation model consisted of a spherical region of 18 Å radius, centered on the position of the adenylate phosphorus, which includes the active site region of HisRS, one ligand molecule (HisAMP, His, HisOH, or His+ATP), and about 325 explicit water molecules solvating the active site. The histidine moiety is neutral, with the Nϵ, which interacts with Glu131, protonated and the Nδ, which interacts with Tyr264, deprotonated. The initial protein and ligand coordinates for the native complexes were taken from the crystal structure of the *E. coli* enzyme: HisAMP complex[4,5] (PDB accession codes 1kmm and 1kmn). The structures of the mutant complexes were built as described below.

Atomic charges, van der Waals, and stereochemical force field parameters for protein and ligand, with the exception of a portion of the adenylate, were taken from the CHARMM22 all-atom force field.[22] Parameters for the central part of the adenylate were derived from quantum chemical calculations, as described in the Appendix. Water interactions were described by a modified TIP3P model,[23,24] which has a dielectric constant of 82.[25] Water molecules were confined within the 18 Å sphere by the stochastic boundary method.[26] Protein atoms within the outer 3 Å buffer shell, *i.e.*, more than 15 Å from the center of the simulation sphere, were harmonically restrained to their initial positions. Unpaired charged side chains (*i.e.*, those not involved in salt bridges) in the buffer region had their charges reduced by a factor of 40, to account for the absence of bulk solvent.[27] Protein and water heavy atoms located more than 15 Å from the center of the sphere were subjected to Langevin dynamics with frictional and random forces that mimic a thermal bath at a chosen temperature.[26] The internal geometry of the water molecules and bond lengths to protein hydrogen atoms were constrained with the SHAKE algorithm.[28] Initial water positions were obtained by overlaying a large box of bulk water on the protein structure and deleting waters that overlap with protein. Each structure was then optimized through Powell minimization,[29] gradually heated to room temperature by molecular dynamics over a period of 30 ps, and then subjected to several hundred picoseconds of molecular dynamics at 293 K. An additional water overlay was done after the first few picoseconds of equilibration, to account for electrostriction of the water around charged protein groups. The coordinates were stored every 20 or 40 fs for further analysis. Energy minimization and molecular dynamics calculations were done with the programs X-PLOR[30] and CHARMM.[31]

All simulations but one were done with a 16 Å cutoff for electrostatic interactions (using a shifting function[31]). The use of even a relatively large cutoff, as here, is a significant approximation. To test its effects, one simulation of the native HisAMP complex was done without any cutoff, *i.e.*, including all electrostatic interactions. This is done efficiently in the CHARMM program by approximating small groups of atoms by sets of electric multipoles when computing interactions beyond 13 Å.[31,32] Because of the good agreement between the HisAMP simulations with and without cutoff (see below), all the other simulations were done with a cutoff.

The crystal structure of HisRS from *T. thermophilus* (HisRStt) is more complete than that from *E. coli*, since it includes the insertion domain,[21] which is disordered in the structure of the enzyme from *E. coli* (residues 188–223). However, its coordinates (released Aug. 20, 1997) only became available after

TABLE I. Residues Mutated in HisRS

	Mutant				
Wild type	1	2	3	4	SerRS
Ile168	—	Lys	—	Lys	Lys327
Arg259	Gly	Gly	Gly	Gly	—
Val268	Gln	Gln	Gln	Gln	Gln330
Glu270	—	—	Asp	Asp	Asp332
Thr281	Asp	Asp	Glu	Glu	Glu345
Ala284	Ser	Ser	Ser	Ser	Ser348

the present simulations had been performed. An a posteriori examination of the HisRStt structure showed that the α-helix containing residues 200–210 is within our 18 Å sphere, occupying space that is filled with solvent in our simulations. The side chain extremities of four residues of the helix extend into the inner 15 Å sphere: the guanidino group of Arg204 (10 Å from Pα), the carboxylate of Asp207 (9.8 Å from Pα), the ammonium of Lys209 (11.9 Å from Pα), and the guanidino of Arg197 (14.7 Å from Pα). The first three are fully solvated, so that their charges are largely shielded from groups in the active site. Arg197 forms a salt bridge to Asp59 (in HisRStt, equivalent to Asp61 in HisRS from *E. coli*) and is sufficiently far away from the phosphate and magnesium to be neglected. Furthermore, all these residues are expected to be relatively disordered based on the low electron density observed experimentally. Hence, including these groups would not be expected to affect the behavior of the active site significantly during the molecular dynamics simulations.

Four sets of mutations were introduced into the wild-type *E. coli* HisRS structure. They are summarized in Table I. In all four cases, Arg259 was changed to Gly, Val268 to Gln, and Ala284 to Ser. Thr281 was changed to a carboxylate, *i.e.*, to Asp in the first two constructs and to Glu in the other two. Glu270 was changed to Asp in the latter two instances. Ile168 was changed to Lys once for each carboxylate combination. A Lys is present at the corresponding position in SerRS (Fig. 1). The coordinates of the mutated residues were built into the native *E. coli* HisRS:HisAMP complex by superimposing atoms shared with the native residues and assuming an ideal stereochemistry for the others. The native complex was taken from the native simulations described above. Only minimal energy optimization was necessary after introduction of the mutated residues, since the model was already pre-equilibrated by the earlier simulations.

The loop 273–281 that anchors the putative Mg^{2+} ligand Asp/Glu281 has two possible conformations in the *E. coli* HisRS:HisAMP crystal structure (Arnez, Francklyn and Moras, unpublished data). The major conformation differs from that of the equivalent loop in SerRS, while the less-populated one is similar to that in SerRS. They will be referred to as the major and minor conformations, respectively. In the minor conformation, residue 281 is closer to the principal Mg^{2+} ion, and in SerRS, the Glu at this position coordinates both the principal and the second Mg^{2+} ions. Exchange between the two conformations is slow on the time scale of the present simulations (200–600 ps). Therefore, both conformations were simulated individually. In the structure of HisRS from *T. thermophilus*,[21] which became available after the simulations were finished, the "minor" conformation of the loop predominates.

Mutants 1–4 were simulated complexed with HisAMP, with the 273–281 loop in its major conformation. Mutants 1 and 3 were also simulated with the 273–281 loop in its minor conformation. Mutant 3, which gave the best results in terms of metal coordination, was examined through three additional simulations. The adenylate was replaced with His alone in one simulation and with His+ATP in two. Additional space made available to solvent in the His complex was filled by overlaying a sphere of water molecules on the system and retaining 12 waters that fit into the available space. In the His+ATP cases, six waters were deleted to avoid overlap with the ATP. The two His+ATP simulations were done with the 273–281 loop in its major and minor conformations, respectively. Each complex was then minimized and underwent 200–300 ps of Langevin dynamics in most cases, or 600 ps in the His+ATP cases.

RESULTS

Native Simulations

The native HisAMP complex was simulated with and without an electrostatic cutoff (see Materials and Methods). The structures sampled in the two simulations were in good agreement with each other and with the crystal structure (Table II). The three structures are compared in Figure 2.

The root-mean-square (rms) deviation between the two simulation structures (averaged over the last 5 ps of simulation) was only 0.4 Å for backbone, 0.7 Å for side chains, and 0.5 Å for the adenylate. The rms deviations between the simulation and experimental structures were 0.7 Å and 0.5 Å with and without cutoff (backbone atoms), or 1.2 Å (side chain atoms, with or without cutoff). These are roughly comparable to the rms deviations between monomers in the crystal structure: 0.2 and 1.3 Å for backbone and side chains, respectively. The imidazole ring is slightly tilted around the χ1 dihedral in the simulations. In the cutoff simulation, a localized distortion occurred due to a 180 degree rotation of the C5' around the α torsion angle of the phosphate group, which displaces the C5' by 1.5 Å and twists the ribose downwards somewhat. This is compensated by rotation around the χ glycosyl torsion angle, so that the distortion is limited to a few atoms, and the most important ligand atoms (*e.g.*, the adenine N9, the P, the carboxyl C, and the imidazole Nδ) are

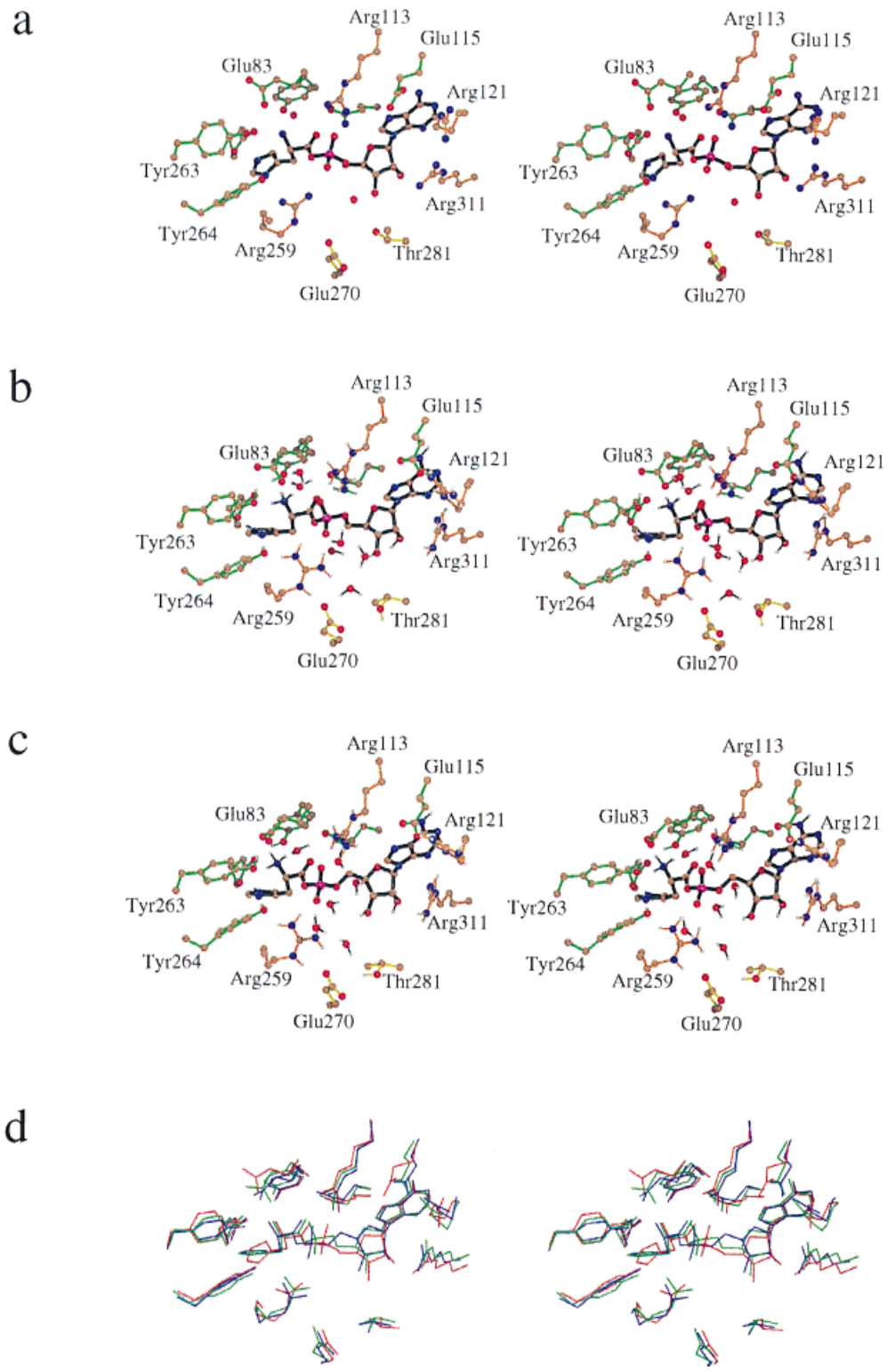

Fig. 2. Stereo views of the active site region of the native HisRS:HisAMP complex. **a:** Crystal structure.[5] **b:** Snapshot after 200 ps of molecular dynamics simulation with no electrostatic cutoff. **c:** Snapshot after a further 200 ps with a 16 Å cutoff for electrostatic interactions. Shown are the ligand, histidyl-adenylate (black bonds), the residues mutated in mutants 1–4 further on (yellow bonds), the three class II conserved arginines (orange bonds), and some other important residues that interact with histidyl-adenylate (green bonds). **d:** Superposition of a, red; b, green; and c, blue.

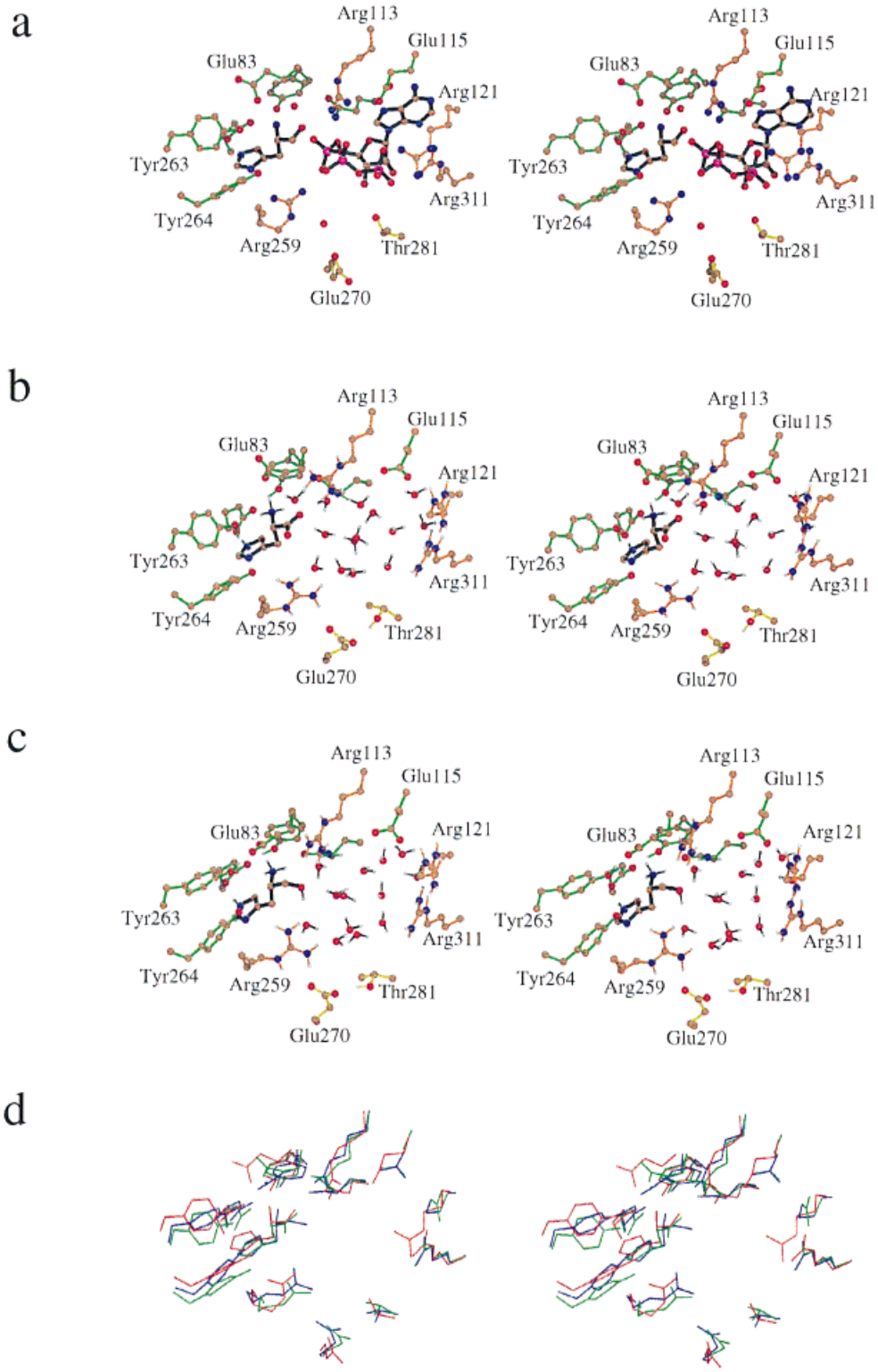

Fig. 3. Stereo views of the active site region of the native HisRS:His and HisRS:HisOH complexes. **a:** Crystal structure of the HisRS:HisOH:ATP complex.[5] **b:** Snapshot of molecular dynamics simulation of HisRS:His. **c:** Idem, HisRS:HisOH. Shown are the ligands (black bonds), the residues mutated in mutants 1–4 further on (yellow bonds), the three class II conserved arginines (orange bonds), and some other important residues that interact with histidine or ATP (green bonds). **d:** Superposition of a, red; b, green; and c, blue.

TABLE II. Magnesium Environment in Different Complexes[†]

Protein Ligand(s) Loop conf.[a]	Native HisAMP major	Mutant 1 HisAMP minor	Mutant 2 HisAMP major	Mutant 3 HisAMP Major	Mutant 3 HisAMP Minor	Mutant 3 His/ATP Major	Mutant 3 His/ATP Minor	Mutant 3 His major	Mutant 4 HisAMP major
Ligand rmsd[b]	0.55	0.46	0.92	0.67	0.49	0.85/1.10	0.81/1.15	0.98	0.70
Ligand rmsf[c]	0.34	0.35	0.33	0.30	0.33	0.17/0.41	0.21/0.43	0.49	0.30
Mg^{2+} rmsd[b]	0.52 (R259)[d]	0.87	1.06	1.53	1.38	1.63	0.18	0.43	1.42
Mg^{2+} rmsf[c]	0.41 (R259)[d]	0.28	0.44	0.26	0.38	0.28	0.29	0.33	0.36
Mg^{2+}-S284[e]	na[f]	2.15 (9)	—	2.21 (8)	—	2.15 (9)	2.20 (10)	2.10 (7)	2.10 (7)
Mg^{2+}-E270	na	1.87 (4)	1.92 (5)	—	—	—	—	—	—
Mg^{2+}-E281	na	—	—	—	1.91 (5)	—	1.91 (4)	—	—
Mg^{2+}-O1P	na	—	1.91 (4)	1.88 (3)	1.89 (3)	1.87 (3)	1.89 (4)/1.91 (4)[h]	na	1.87 (3)
Mg^{2+}-water	na	2.02–2.03 (4)[i]	2.02–2.04 (4)	2.02–2.03 (4)	2.03–2.04 (4)	2.01–2.03 (4)	2.03 (4)	2.02–2.03 (4)	2.01–2.04 (4)
No. of waters[g]	na	4	4	4	4	4	2	5	4
R113-OxP[j]	2.70 (12)	3.17 (71)	—	2.73 (11)	2.70 (10)	2.75 (14)	—	na	3.77 (25)
Y264-N_δ[k]	1.91 (11)	2.02 (20)	—	1.88 (11)	2.20 (43)	1.92 (12)	1.90 (11)	1.92 (12)	1.91 (11)

[†]All distances in Å.
[a]Conformation of the 273–281 loop (major or minor; see text).
[b]rms deviation at the end of the simulation from starting structure.
[c]rms fluctuation around mean structure.
[d]Result for R259 side chain charge.
[e]Distance from Mg^{2+} to the nearest atom of ligating group (S284-O_γ, E270-O_ϵ, E281-O_ϵ, O1P, water oxygen). Standard deviation in parentheses expressed in significant digits. When the group is too far to coordinate the ion, "—" is indicated.
[f]Group not present.
[g]Number of waters coordinating Mg^{2+}.
[h]The Mg^{2+} bridges the α- and β-phosphate groups, each of which coordinates the ion with an O1P atom; both distances are reported.
[i]Range of distances corresponding to the different coordinating waters.
[j]Distance between Arg113-H_η and the nearest phosphate oxygen.
[k]Distance between Tyr264-OH and imidazole N_δ.

all correctly positioned, with shifts of just 0.3–0.4 Å (Fig. 2d). The experimental 3'-endo sugar pucker is preserved in all cases. Moreover, all the main adenylate interactions observed experimentally are preserved in both simulations. The HisAMP imidazole group hydrogen bonds to Glu131 in the back of the binding pocket and to Tyr264 in the front. Tyr264 is anchored in place by a hydrogen bond to Arg259, which also hydrogen bonds to the adenylate α-phosphate and to Glu270 below. The ammonium group of the His moiety of HisAMP hydrogen bonds to Thr85, Glu83, and a stable water molecule. This water fills a cavity in the back of the binding pocket, bridging the ligand ammonium, the Gln127 amide group, and the Tyr107 hydroxyl; it is seen in the same position in the crystal structure. The adenylate phosphate also interacts with the motif 2 Arg113 and (more weakly) with Gln127, and the adenine moiety stacks on the conserved Phe125. This active site network is very stable, as indicated by the small atomic fluctuations about their mean positions (0.3–0.5 Å for all atoms; Table II) and the stability of the hydrogen bonds mentioned (90–100% occupancy over 2 × 200 ps).

In the simulation of the His complex, the interactions of the amino acid are very similar to those outlined above and to the crystal structure of the HisRS:HisOH:ATP complex (Fig. 3). A typical snapshot from the simulation is shown in Figure 3b. The imidazole is tilted downwards slightly around χ1, on average, in the opposite direction from the adenylate simulations. However, the hydrogen bonds to Glu131 and Tyr264 are preserved, and the ammonium makes the same interactions as before. The main differences are around the carboxylate group. This group interacts with Arg113 through a bridging water molecule; hydrogen bonds to Gln127 and Arg259 are present initially, but break after about 120 ps as the carboxylate becomes solvated. In the HisOH complex (Fig. 3c), the ligand is shifted almost 1 Å further back into the binding pocket. In a simulation where His starts out in the HisOH position, the opposite shift is observed (not shown). This shift appears to be driven by optimization of the interactions of the HisOH ammonium, given that the constraint to maintain strong interactions between the His carboxylate group and water or arginines is removed. Arg259 does not hydrogen bond to histidinol at all, and its hydrogen bond to Tyr264 is only present 20% of the time. The rest of the time it is solvated. The histidinol hydroxyl interacts with water. Compared with the crystal structure of HisRStt, both the His and HisOH are shifted by 1 Å and rotated slightly; all three imidazole rings are nearly superimposable.

Mutants 1–4 Complexed With HisAMP

As described in Materials and Methods, the 273–281 loop occupies two distinct conformations in native HisRS, which place the carboxylate side chain of residue 281 in two different positions with respect to the α-phosphate and the putative Mg^{2+} site. Since this carboxylate coordinates the principal Mg^{2+} in SerRS, it is important to investigate both loop conformations explicitly. We first describe simulations of all four mutants in complex with HisAMP with the 273–281 loop in its major conformation (the predominant conformation in *E. coli* HisRS, as seen in the crystal structure). Simulations with the loop in its

minor conformation are described further on. All four mutants behaved stably throughout the simulations, as illustrated by the small rms deviations of the structures from their starting positions (Table II). These values ranged from 1.1 to 1.2 Å for all atoms, from 0.7 to 0.9 Å for the backbone, and from 0.7 to 1.0 Å for the HisAMP. The rms fluctuations around the mean structure for the heavy atoms inside the unrestrained simulation region are 0.32–0.39 Å for the HisAMP complexes. Slightly larger fluctuations are observed below with the His and His+ATP complexes, 0.36–0.40 Å. These are similar to the value observed in recent simulations of an Asp-AspRS complex, 0.42 Å.[33] The final resulting coordinates from each simulation are shown in Figure 4.

Data pertaining to the Mg^{2+} coordination and substrate deviations are summarized in Table II. In the mutant complexes, the adenylate has only slightly larger deviations from its starting position than in the native simulations, and similar rms fluctuations. The interactions of the ligand imidazole were largely preserved in all cases. However, the Mg^{2+} coordination sphere underwent some rearrangements in each case.

Mutant 1 (R259G, T281D, A284S, V268Q, Fig. 4a) has shifted from the starting structure by an rms deviation of 1.2 Å for all heavy atoms and 0.9 Å for the adenylate. In the starting structure, the Mg^{2+} ion is coordinated to Ser284, Glu270, and the α-phosphate of the adenylate. The remaining Mg^{2+} coordination sites are occupied by water molecules. The 273–281 loop is in its major conformation, and Asp281 is too far away to coordinate the Mg^{2+} directly (unlike the equivalent Glu in SerRS). Within the first 20 ps, the Mg^{2+} ion shifts 1.5 Å left- and downwards, losing its coordination to the α-phosphate, but remaining coordinated to Ser284 and Glu270 and to four waters. After the initial shift, the structure is mostly stable, as shown by the lack of drift of the ion (not shown) and the small fluctuations of the Mg^{2+}-ligand distances (Table II). One of the Mg^{2+}-coordinated waters interacts with Asp281 and two of them form bridges to the α-phosphate. Ser284 hydrogen bonds part of the time to the α-phosphate and part of the time to a water molecule that interacts with Tyr264. Tyr264 does not interact directly with any of the Mg^{2+}-coordinated water molecules. Arg113 interacts directly with the α-phosphate most of the time, although the two are occasionally bridged by water molecules.

Mutant 2 (R259G, T281D, A284S, V268Q, I168K, Fig. 4b) has shifted from the starting structure by an rms deviation of 1.2 Å for heavy atoms and 1.0 Å for the adenylate. The Mg^{2+} ion has the same initial cooordination as mutant 1. Within the first 20 ps, the coordination sphere rearranges. The Mg^{2+} remains coordinated to Glu270 and the α-phosphate of the adenylate, but not to Ser284. The remaining Mg^{2+} coordination sites are occupied by water molecules, one of which interacts with Asp281. The coordination sphere is distorted and not as good as that in the other mutants. The α-phosphate has shifted 1 Å downwards, losing its direct interaction with the class II Arg113, which becomes mediated by two water molecules. Ser284 donates its hydrogen bond alternately to Glu270 and to the α-phosphate of the adenylate. Lys168, which is only present in mutants 2 and 4 (Table I), appears to orient Gln268 such that the latter interacts with Glu270. This places Glu270 in a different orientation with respect to the metal ion, compared with the mutant 1 simulation; this may play a role in enabling the Mg^{2+} ion to coordinate the α-phosphate directly. Tyr264 donates its hydrogen bond to Ser284 instead of to the Nδ of the His moiety; the latter interacts with a water molecule instead.

Mutant 3 (R259G, E270D, T281E, A284S, V268Q, Fig. 4c) has shifted from the starting structure by an rms deviation of 1.3 Å for heavy atoms and 0.7 Å for the adenylate. In the starting structure, the Mg^{2+} ion is coordinated to the α-phosphate, Ser284, three waters, and Glu281. Asp270 is too short to coordinate the ion directly and interacts through a water molecule instead. Although the 273–281 loop is in its major conformation, Glu281 reaches far enough to coordinate the ion when it is built in a fully extended conformation. Within the first 20 ps of simulation, however, Glu281 bends back and a water molecule becomes inserted between it and the Mg^{2+} ion. The ion remains coordinated to Ser284 and the α-phosphate of the adenylate. The remaining Mg^{2+} coordination sites are occupied by water molecules, one of which interacts with Glu281 part of the time. After the initial rearrangement, the coordination sphere is very stable throughout the simulation, with the lowest rms fluctuation and no significant drift, although the rms deviation from the starting structure is the highest of the four mutants (Table II). The rms fluctuation of the histidyl-adenylate and its rms deviation from the starting structure are also the lowest. Ser284 interacts with Asp270, which presumably helps to fix the Ser284 orientation and stabilizes its interaction with the Mg^{2+}. Another Mg^{2+}-coordinated water molecule donates a hydrogen bond to the phenolic OH of Tyr264, which in turn hydrogen bonds to the Nδ of the histidine moiety of the adenylate. The class II Arg113 interacts directly with the α-phosphate as in the native structure.

Mutant 4 (R259G, E270D, T281E, A284S, V268Q, I168K, Fig. 4d) behaves similarly to mutant 3. After 200 ps, it has shifted from the starting structure by an rms deviation of 1.1 Å for heavy atoms and 0.7 Å for the adenylate. The initial Mg^{2+} coordination is the same as for mutant 3. After 20 ps of simulation, the Mg^{2+} is coordinated to Ser284 and the α-phosphate of the adenylate, but not to Asp270 or Glu281, which

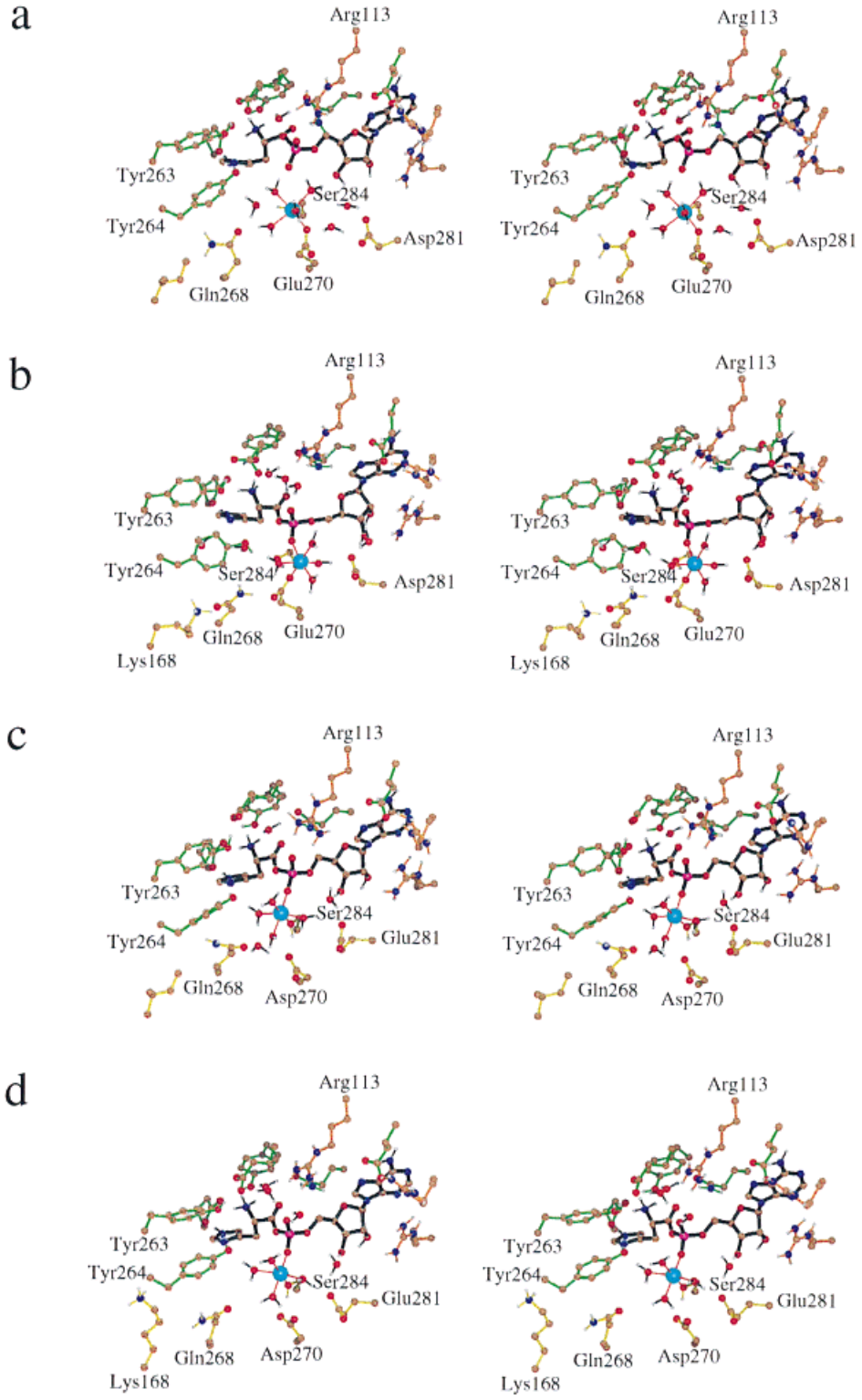

Fig. 4. Stereo views of the active site region of mutant HisRS:HisAMP complexes after 200 ps of molecular dynamics simulations. **a:** Mutant 1: R259G, T281D, A284S, V268Q. **b:** Mutant 2: R259G, T281D, A284S, V268Q, I168K. **c:** Mutant 3: R259G, E270D, T281E, A284S, V268Q. **d:** Mutant 4: R259G, E270D, T281E, A284S, V268Q, I168K. Shown are the ligand, histidyl-adenylate (black bonds), the mutated residues (yellow bonds), the three class II conserved arginines (orange bonds), and some other important residues that interact with histidyl-adenylate (green bonds). The metal ions are drawn as light blue spheres.

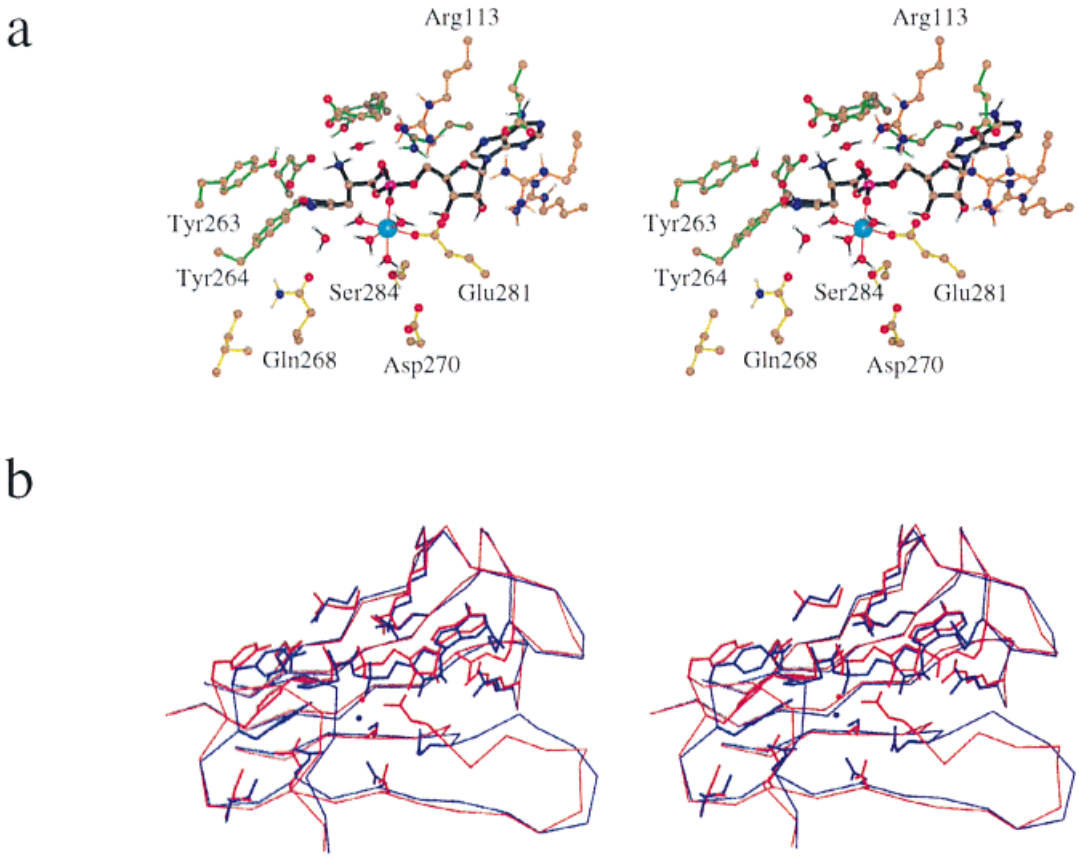

Fig. 5. Stereo views of (**a**) the active site of mutant 3 HisAMP complex from the simulation with the minor 273–281 loop conformation and (**b**) comparison of the simulations of the mutant 3 HisAMP complex with the major (blue) and minor (red) loop conformation.

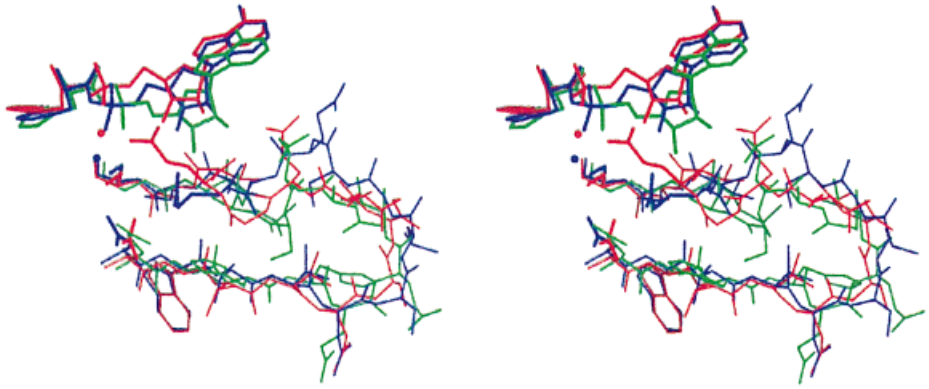

Fig. 6. Alternative 273–281 loop structures. Stereo views of the major (blue) and minor (red) loop conformations in mutant 3:HisAMP and HisRS from *T. thermophilus* (green).

has bent away as before. The remaining Mg^{2+} coordination sites are occupied by water molecules, one of which occasionally interacts with Glu281 and another hydrogen bonds with Asp270. Ser284 also interacts with Asp270. The coordination sphere is very stable through the dynamics simulation. Much as in mutant 3, another Mg^{2+}-coordinated water molecule donates a hydrogen bond to the phenolic OH of Tyr264, which in turn donates its hydrogen bond to the Nδ of the histidine moiety of the adenylate. Lys168 does not seem to play any role in the active site; instead, it interacts with the backbone carbonyl oxygen of Tyr264 and otherwise faces the solvent. Arg113 contacts the α-phosphate directly but weakly (average O2P-Nη distance of 3.8 Å, compared to 2.7 Å in mutant 3).

Mutants 1 and 3 Complexed With HisAMP With the 73–281 Loop in its Minor Conformation

The question arises why Glu281 in the simulations of mutants 3 and 4 does not maintain a conformation similar to that of its homologue Glu345 in SerRS, which coordinates the principal metal ion. The "major" conformation of its anchoring loop 273–281 is different from that in SerRS, and in HisRS from *T. thermophilus*, as discussed. The loop started out in this conformation and did not undergo any significant rearrangements during the simulations. With this backbone conformation, Glu281 can only coordinate Mg^{2+} in a completely extended conformation. The ability of the loop to adjust during the simulations may be limited because the backbone of residues 275–276 is in the outer part of the simulation model and was constrained during the calculations. Despite the constraints, a significant portion of the loop was in the inner 15 Å free dynamics sphere, and so it was free in principle to adjust in order to optimize the Glu281 position. However, the simulation length may be insufficient for this to occur. Therefore, to address the effect of loop conformation on the Mg^{2+} coordination, additional simulations of mutants 1 and 3 were performed. The 273–281 loop was rebuilt into the weak experimental electronic density that represents the minor loop conformation in the native structure. This alternate conformation is close to that of the homologous loop in SerRS. In this geometry, Glu281 of mutant 3 initially coordinates the principal Mg^{2+}, while Asp281 of mutant 1 interacts through a water molecule. Simulations were then initiated from this starting conformation. The two loop conformations are compared in Figure 5. The mutant 1 and 3 simulations are expected to be approximately representative of mutants 2 and 4, as well. Indeed, mutant 4 behaves very similarly to mutant 3 in the simulations above and has the same side chain (Glu) at position 281. Mutant 2 has the same side chain (Asp) as mutant 1, which is too short to directly coordinate the Mg^{2+}, even with the loop in its minor conformation (see below).

Within the first 20 ps of the mutant 1 simulation, the loop conformation relaxes into a structure very similar to the major conformation occupied in the previous simulation. The resulting active site structure is intermediate between those of mutants 1 and 2 in the previous simulations. The Asp281 side chain is 2 Å from its position in the previous mutant 1 simulation, and only 1 Å from its position in the mutant 2 simulation. The overall rms deviations from the previous mutant 1 and 2 simulations are 0.6 and 0.8 Å, respectively, for non-hydrogen atoms within 6 Å of the ligand. The Mg^{2+} coordination is very similar to the previous mutant 2 simulation and differs from the previous mutant 1 simulation, with Ser284, Glu270 and the α-phosphate interacting directly with the ion. Asp281 interacts through a water molecule, and the α-phosphate is separated from the class II Arg113 by a water molecule, as in mutant 2.

The rearrangements described above do not appear to be strongly dependent on the loop reconstruction, since the structures sampled are similar to mutant 1 and 2 structures with the major loop conformation; rather, they probably reflect an alternate stable arrangement sampled as a result of slightly different initial conditions. It appears that the main factor influencing the Mg^{2+} coordination in mutants 1 and 2, and differentiating it from mutants 3 and 4, is the nature of the 270–281 carboxylate pair: (Glu-Asp). If so, the structures sampled in this simulation and the previous mutant 1 and 2 simulations can be viewed as alternate possible arrangements of the active site for this carboxylate sequence. The magnitude of the rearrangements between the three simulations then gives a measure of the uncertainty of the simulation model, with respect to the exact geometry of the active site.

In the mutant 3 simulation, the effect of the changed loop conformation is also small. A typical snapshot of the structure is shown in Figure 5a, and the structure is compared with the previous mutant 3 simulation in Figure 5b. A detailed comparison of the loop regions is shown in Figure 6.

The main differences from the previous mutant 3 simulation are the replacement of a water in the Mg^{2+} coordination sphere by Glu281, a downward shift of the α-phosphate and the Mg^{2+} by 1 Å, and a rotation of the coordination sphere so that Ser284 now interacts through a water molecule. The rms deviation from the starting structure is reduced from 1.3 Å to 0.9 Å (nonhydrogen atoms; Table II), and the average potential energy is reduced by 42 kcal/mol, or 1.4 standard deviations, compared with the major loop conformation (-5,373 vs. –5,331 kcal/mol). These results suggest that the present structure may be the more stable. The Mg^{2+} fluctuations are increased from 0.28 Å to 0.38 Å, but the fluctuations of the ion-ligand distances are of the same magnitude as previously. The range of active site fluctuations is illustrated by a series of snapshots in Figure 7a. The waters coordinating the ligand ammonium and the Mg^{2+} are seen to be very stable, typical of all the simulations.

Mutant 3 in Complex With His and His+ATP

Mutant 3 was selected for further study, since its Mg^{2+} ion coordination most closely matches that of the equivalent ion in SerRS.[6] In addition, Tyr264 accepts a hydrogen bond from the Mg^{2+}-hydrate, which in this case plays the role of Arg259 in the wild-type HisRS.[5] This in turn enables Tyr264 to donate its phenolic proton to the Nδ of the histidine moiety of the adenylate and thus participate in the specific recognition of the imidazole group. By con-

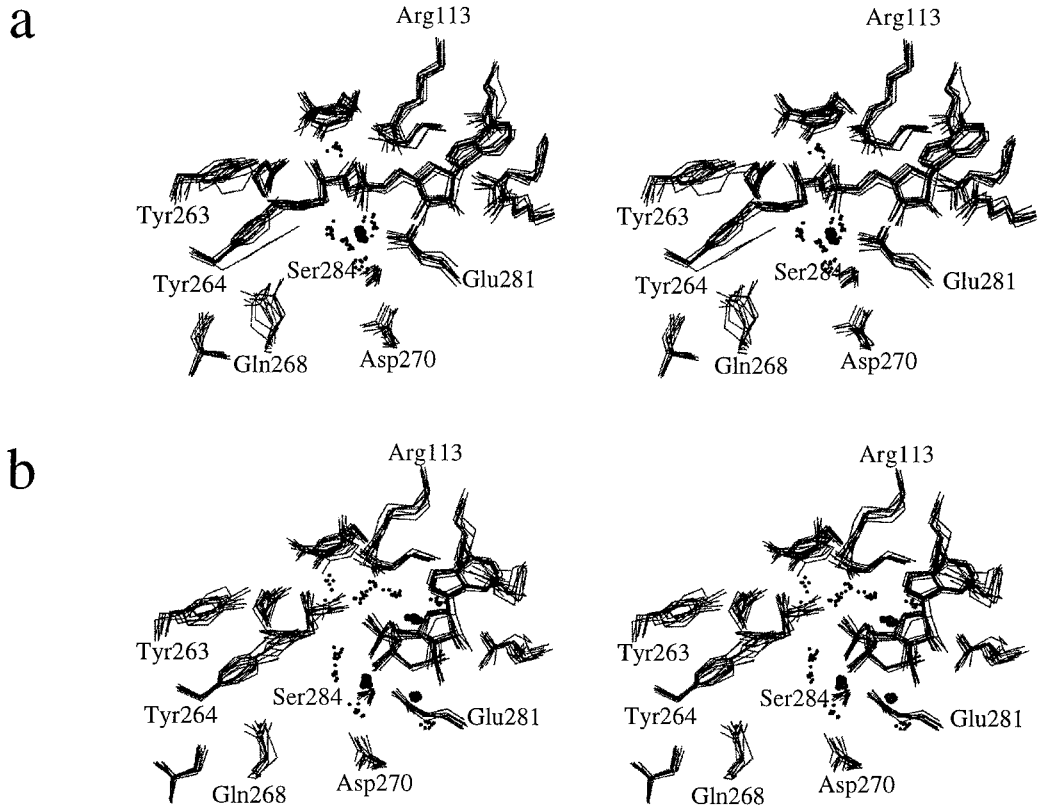

Fig. 7. Stereo views of ten snapshots at 10 ps intervals of the active site region of mutant 3 (minor loop conformation) complexed (**a**) with histidyl-adenylate and (**b**) with histidine and ATP. Shown are the ligand(s), the mutated residues, the three class II conserved arginines, and some other important residues that interact with histidine and ATP, the metal ions, and selected waters coordinating the principal Mg^{2+} and the ligand ammonium. Waters are shown as small spheres.

trast, in mutant 2 and occasionally in mutant 1, Tyr264 does not fill this role as effectively. Two molecular dynamics simulations of mutant 3 complexed with His+ATP were therefore performed, with the 273–281 loop initially in its major and minor conformations, respectively. These simulations lasted 600 ps each, and for the last 400 ps all constraints on the 273–281 loop (*i.e.,* on residues 275–276 in the outer buffer region) were removed so that the loop was free to adjust its conformation. Even so, no significant loop rearrangements were seen in either His+ATP simulation. The principal Mg^{2+} occupies different positions in the two simulations, as described below. A single simulation of mutant 3 complexed with His was also performed.

In the His+ATP complex with the major loop conformation, Glu281 was initially built in an extended conformation, coordinating the principal Mg^{2+}. It shifted away within 20 ps of dynamics as before, to be replaced by a water molecule. The coordination sphere of the principal Mg^{2+} includes the ATP α-phosphate, Ser284, and four waters, only approximately matching that observed in the experimental SerRS:ATP structure. A typical snapshot from the simulation is shown in Figure 8a. The ion-ligand distances are very stable as a function of time (Fig. 9a). The main differences with SerRS are the missing Glu281 coordination and a 1.5 Å shift of the ion towards the α-phosphate in the simulation; in SerRS, the ion bridges the α- and β-phosphates. Nevertheless, comparing the present reactant simulation with the corresponding product (*i.e.,* HisAMP) simulation above, the active site appears preorganized to carry out the adenylation reaction. For example, the principal Mg^{2+} ion and the reactive Pα are shifted by just 1 and 2 Å, respectively, compared with the corresponding HisAMP simulation. A 1 Å Mg^{2+} shift was recently observed experimentally between the equivalent states in GlyRS (Arnez, Dock-Bregeon, and Moras, in preparation). The His carboxylate interacts directly with the principal Mg^{2+} hydrate, while the (ATP)Pα-OT(His) distances fluctuate around 4 Å and frequently reach values of less than 3.5 Å (Fig. 9b). The Mg^{2+} hydrate continues to orient properly Tyr264, which maintains its specific interaction with the imidazole group. Arg113 interacts directly with the α-phosphate for the first 500 ps, and then shifts away slightly so that the interaction becomes mediated by a water molecule. One of the remaining Mg^{2+} ions bridges the β- and

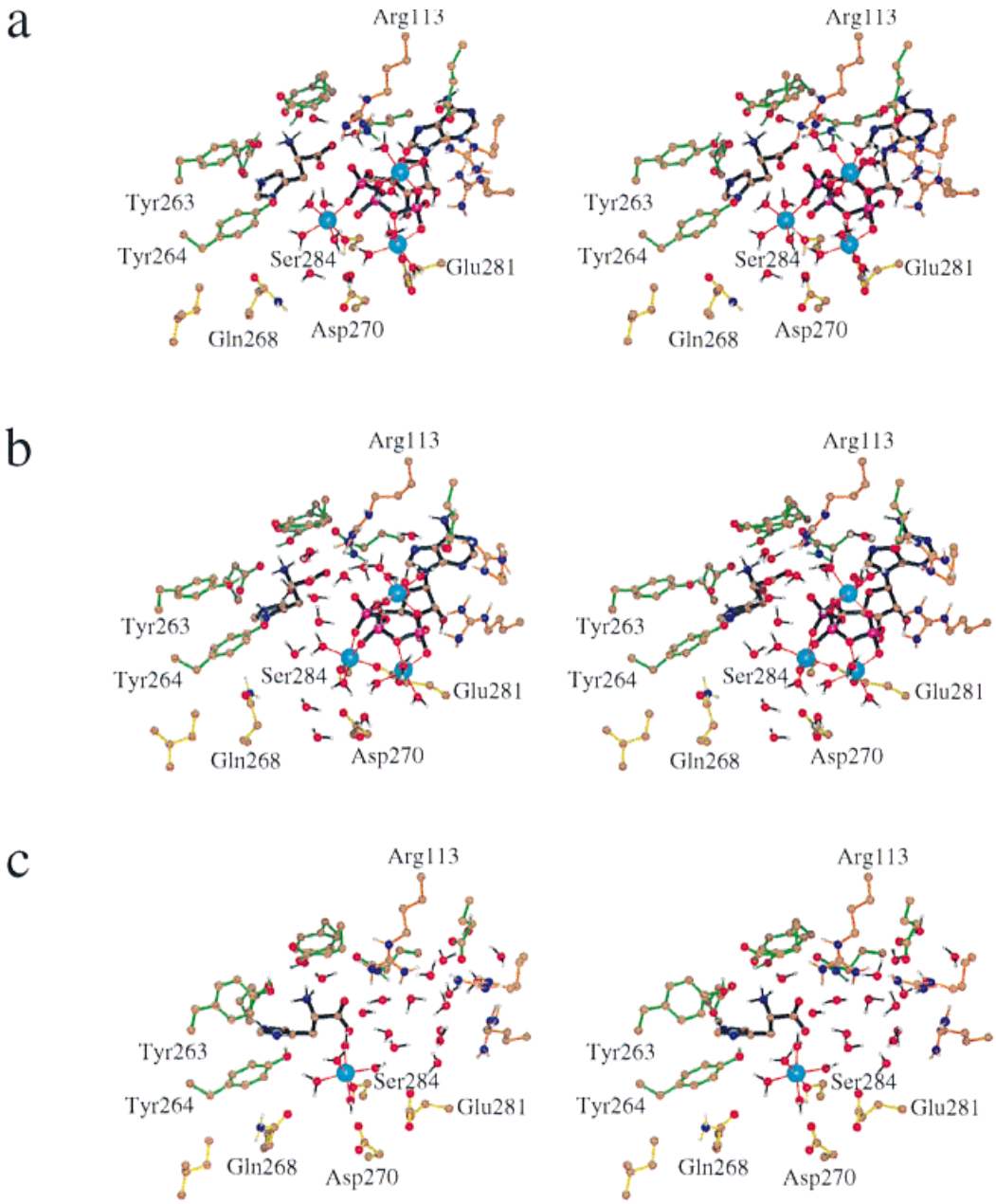

Fig. 8. Stereo views of the active site region of mutant 3 complexed (**a**) with histidine and ATP, with the 273–281 loop in its major conformation; (**b**) with the same, but in the minor loop conformation; (**c**) with His alone. Shown are the ligand(s) (black bonds), the mutated residues (yellow bonds), the three class II conserved arginines (orange bonds), and some other important residues that interact with histidine and ATP (green bonds). The metal ions are drawn as light blue spheres.

γ-phosphates, with the other coordination sites filled by water molecules. These waters hydrogen-bond to Glu66 and Glu115. The former is invariant among prokaryotic HisRS, and the latter is highly conserved in class II aaRSs (being part of motif 2).[4] The third ion coordinates the γ-phosphate; this differs from the coordination geometry observed in SerRS (bridging the β- and γ-phosphates)[6] or HisRS (mostly on the β-phosphate).[5] Glu281 is coordinated to the latter Mg^{2+} and also occasionally interacts with a water molecule that is coordinated to the principal Mg^{2+}. All three Mg^{2+} ion sites are highly stable throughout the 600 ps simulation (Fig. 9a).

In the His+ATP complex with the minor loop conformation, the Mg^{2+} coordination sphere matches that of SerRS more closely: the principal Mg^{2+} bridges the α- and β-phosphates as in SerRS, while the other coordination sites are occupied by Ser284, two waters, and Glu281, which consistently coordinates both the principal and the third Mg^{2+} ions. A

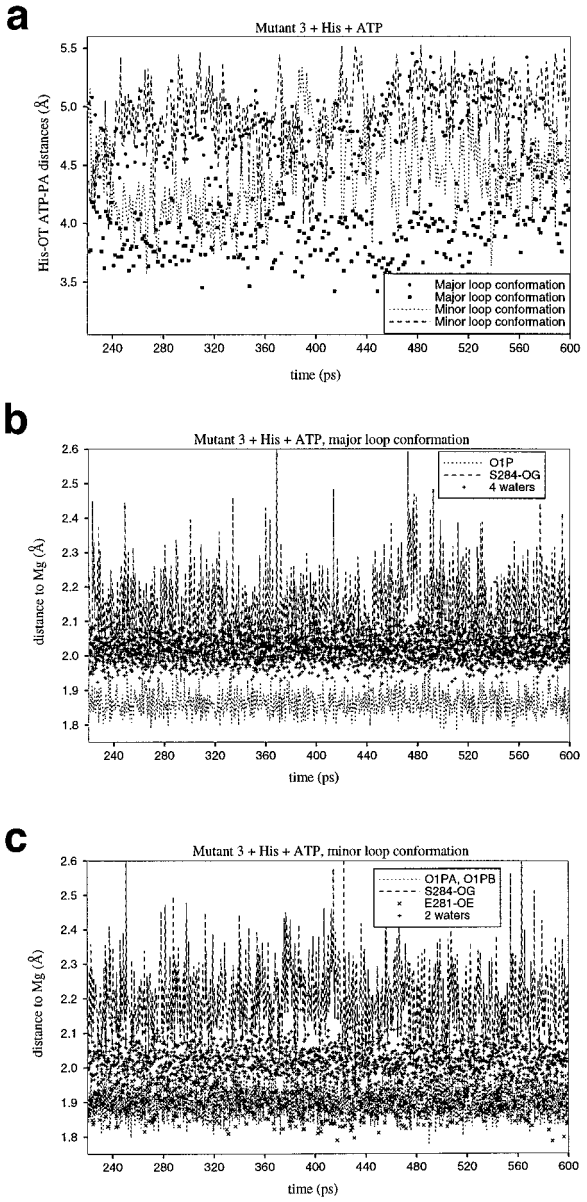

Fig. 9. Selected interatomic distances as a function of time. Distances between (**a**) the carboxylate oxygens OT1 and OT2 of His and the **α**-phosphorus of ATP; and (**b**) and (**c**) between the principal Mg^{2+} ion and its ligands, as indicated: one or two of the **α**-phosphate oxygens, the O**γ** of Ser284, a carboxylate oxygen O**ϵ** of Glu281, and 2–4 water oxygens, with the 273–281 loop in its (b) major and (c) minor conformations.

typical snapshot from the simulation is shown in Figure 8b, and a series of snapshots illustrating the range of fluctuations are shown in Figure 7b. The simulation and SerRS:ATP structures are compared in Figure 10.

The principal Mg^{2+} in the simulation is just 0.7 Å away from its position in SerRS. The main difference with the SerRS active site is a weaker interaction here between the α-phosphate and the class II Arg113, which is mediated by a water molecule throughout the simulation. The rms deviation between the structures sampled in the two simulations is 0.6 Å for non-hydrogen atoms within 6 Å of the ligands. The (ATP)Pα-OT(His) distances are about 0.5 Å longer than in the previous simulation (Fig. 9c), and the His carboxylate is slightly farther from the Mg^{2+} hydrate. The shift between the present His+ATP reactant complex and the corresponding HisAMP product complex is comparable to above. For example, the principal Mg^{2+} shifts by 1.9 Å and the Pα by 1.5 Å. The average potential energy of the present structure is significantly lower than that in the previous simulation with the major loop conformation (-7,423 vs. –7,250 kcal/mol), the difference being five times the standard deviation (ca. 35 kcal/mol). The protein structure also remains closer to its starting structure than in the previous simulation, with an average rms deviation of 1.0 Å for nonhydrogen atoms vs. 1.2 Å above (Table II). This is similar to the HisAMP case above. These results suggest that the present structure is more stable than that sampled with the major loop conformation, and more representative of the mutant 3 His+ATP complex. The other two Mg^{2+} ions occupy essentially the same positions in the simulations with the major and minor loop conformations, and have very similar coordination spheres.

A single His simulation was performed, with the 273–281 loop in its major conformation. Despite the absence of ATP, the principal Mg^{2+} remains in essentially the same position as in the His+ATP simulation above with the major loop conformation (Fig. 8a,c). The interaction with Ser284 is maintained, the α-phosphate is replaced by a water molecule, and the orientation of the five coordinating waters is very close to that observed with His+ATP. Thus, the His carboxylate is pre-positioned to interact with the ATP α-phosphate. Although the minor loop conformation was not simulated for the His complex, we expect that rebuilding the loop in its minor conformation will not modify the Mg^{2+} coordination strongly. In the mutant 3 HisAMP simulations above, the main effect of rebuilding the loop was to replace a water ligand by Glu281, without perturbing the other ligands.

DISCUSSION

In the course of the four native simulations, all complexes studied have dynamically stable structures and interactions with the ligands. The active site structure was observed to be robust with respect to the exact treatment of electrostatic interactions, by comparing simulations with and without an electrostatic cutoff. The structures sampled were in good agreement with the available experimental structures. The amino acid position is essentially the same in the His and HisAMP simulations, indicating that this position is selected prior to ATP binding. The catalytic carbon of His is within 0.75 Å of its

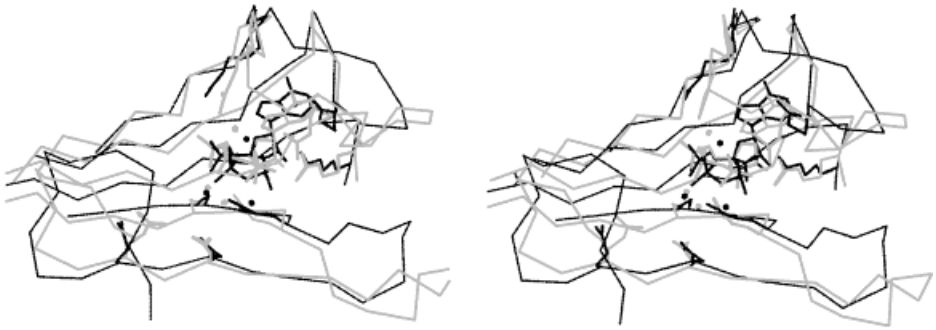

Fig. 10. Stereo view of the superposition of the active sites of HisRS mutant 3 (loop 273–281 in the minor conformation, black) and SerRS[6] (gray), both complexed with ATP.

experimental position in three of four native simulations, and 1.2 Å away in the HisOH simulation. The same preorganization was observed for the Asp substrate in AspRS in X-ray structures at 100 K[34] and molecular dynamics simulations at room temperature.[33] No significant alternate structures around the His moiety were sampled during the native or mutant trajectories. A similar stability (and similar rms atomic fluctuations) was observed in simulations of AspRS complexed with Asp, but not with Asn, where many alternate structures were found over a similar time scale.[33] Some rearrangements occur here during equilibration. For example, HisOH, initially placed in the His position, shifts 1 Å further back into the active site pocket, and His, if initially placed in the HisOH position, shifts outwards by the same amount. These data suggest that the simulation duration was adequate to study the structure of the imidazole binding site. A similar 1 Å shift of HisOH compared with the histidine moiety of HisAMP was observed experimentally.[5]

The mutant simulations illustrate some of the possibilities and limitations of computer experiments for metalloprotein design. Despite the simplicity of the molecular mechanics description, both the octahedral geometry of the Mg^{2+} coordination sphere and the Mg^{2+}-ligand distances (reported in Table III) are in good agreement with those observed in the relevant SerRS, AspRS, and HisRS crystal structures. Similar agreement has been found in nucleic acid simulations,[35] confirming that the Mg^{2+}-phosphate geometry is well reproduced by the force field. The CHARMM22 force field is also known to reproduce the solvation structure around Mg^{2+} in bulk water (A. MacKerell, personal communication). Water-ion distances are slightly shorter here (2.01—2.04 Å) than in bulk water (2.1 Å)[36]; this could be due to slightly stronger electrostatic interactions in the HisRS active site compared with high-dielectric bulk water. Electronic polarization induced by the divalent Mg^{2+} ion in its environment is not explicitly included in the force field; however, the effect of electronic polarizability on the structure and energetics of Mg^{2+}-water clusters has been shown to be small.[37] The CHARMM22 force field has also been used successfully to study zinc binding by several proteins,[32] yielding a zinc coordination sphere in good agreement with experiment, despite the neglect of explicit electronic polarizability. These results suggest that the Mg^{2+} parameters are adequate for the present study.

TABLE III. Mg^{2+} Ion-Ligand Distances†

	AspRS:AspAMP crystal	HisRS mutant 3:HisAMP
Ser	NA (Gly)	(3.74)
Glu	2.46	1.90
OxP	2.33	1.84
H_2O	NA	2.01–2.05
	SerRS:ATP crystal	**HisRS mutant 3:His:ATP**
Site 1		
Ser	2.07	2.12
Glu	2.29	1.91
OαP	2.18	1.90
OβP	2.09	2.01
H_2O	2.21	2.01–2.03
Site 2		
Glu	2.45	1.96
OβP	2.94	1.97
OγP	2.39	1.88
H_2O	2.09	2.01–2.12
Site 3		
OβP	2.27	1.84
OγP	2.34	1.88
H_2O	2.09	2.03–2.06

†The HisRS mutant 3 data are for that with the minor loop conformation.

In the nine mutant simulations, the coordination sphere of the engineered Mg^{2+} sampled several alternate arrangements, which correlate with the nature of the carboxylates (Asp or Glu) at positions 270 and 281, and with the conformation (major or minor) of the 273–281 loop, which anchors residue 281. Indeed, the presence of Glu281 in the coordination sphere depends on the loop conformation. When the 273–281 loop is built in its major HisRS conforma-

tion, neither an Asp nor a Glu at position 281 are close enough to coordinate the engineered Mg^{2+} ion directly in a stable fashion, although they coordinate it indirectly through a bridging water part of the time. When the 273–281 loop is built in its minor, alternate conformation similar to the conformation of the analogous loop in SerRS, Glu281 coordinates the ion directly in a stable fashion. The simulations were unable to select spontaneously between these two loop conformations, as a consequence of the finite simulation length.

Three different positions of the principal Mg^{2+} are seen in the simulations. In mutants 1 and 2 (which have the carboxylate pair Glu270-Asp281), the ion is in a downwards position: it initially coordinates the α-phosphate directly, but during equilibration it shifts downwards to strengthen its interaction with Glu270. In mutant 1 with the major loop conformation, it becomes separated from the α-phosphate by a water molecule. In mutant 2, and mutant 1 with the minor loop conformation, the α-phosphate shifts along with the ion and loses its direct interaction with the class II Arg113, which becomes water-mediated. In mutants 3 and 4 (which have the carboxylate pair Glu270-Asp281), the ion is usually in an upwards position. It coordinates the α-phosphate directly and Asp270 through a bridging water molecule. The other ligands are Ser284, 3 to 4 waters, and in one case Glu281. Finally, in the mutant 3 His+ATP simulation with the minor loop conformation, the principal Mg^{2+} shifts into a third position, between the α- and β-phosphates, very similar to the experimental SerRS:ATP complex. In contrast, with the major loop conformation the Mg^{2+} remains close to the α-phosphate and does not coordinate the β-phosphate.

The positions of the other two Mg^{2+} ions in the ATP complexes are not significantly different in the mutant 3 structures with either the major or the minor loop conformation. One of them coordinates the β- and γ-phosphates and a water molecule that hydrogen bonds to a conserved motif 2 Glu. This is very similar to the Mn^{2+} coordination observed in the crystal structures of the SerRS:ATP and HisRS:ATP complexes. The other metal ion's coordination is more idiosyncratic. In the SerRS:ATP complex it bridges the β- and γ-phosphates; in the crystal structure of the HisRS:HisOH:ATP complex it coordinates the β-phosphate, and in the simulations it coordinates the γ-phosphate. In SerRS and the mutant 3 HisRS simulation it also coordinates the nearly invariant carboxylate.

Among the alternate structures sampled with the different mutants, ligands, and loop conformations it is difficult to predict unambiguously the most stable and catalytically favorable arrangement. Mutant 3 presents the Mg^{2+} coordination most similar to SerRS, particularly when the 273–281 loop is in its minor, SerRS-like conformation. The lower potential energy of this loop conformation and the smaller deviations from the starting structures suggest that this conformation is the most stable for mutant 3. A high degree of preorganization of the catalytic groups is observed when one compares the mutant 3 reactant and product complexes (HisRS:His:ATP and HisRS:HisAMP), as well as the His complex (simulated only with the major loop conformation). For example, the His carboxylate approaches the ATP-Pα within 3.5–3.7 Å several times during the mutant 3 reactant state simulations, and the principal Mg^{2+} ion position differs by 1.9 Å between the reactant and product states. A 1 Å shift was observed experimentally recently in the corresponding GlyRS complexes (Arnez, Dock-Bregeon and Moras, unpublished data).

The results described here show that the Asp-Glu arrangement, in this order (as in Asp270-Glu281), is preferable to the Glu-Asp alternative for coordinating the metals in the active site. This could explain why this sequential arrangement has been observed in most class II aaRSs examined, including AspRS,[9,10] SerRS,[6] and GlyRS.[38] Two class II aaRSs have different residues at the first position: LysRS,[39] which harbors a Glu, and PheRS,[40] which harbors a Gln. This indicates that the second carboxylate is more strictly conserved, with the notable exception of HisRS,[4,5] where the position is occupied by Thr. The first carboxylate in wild-type HisRS is Glu270.

We expect that all four mutant constructs considered here would be stable at the protein structure level. It is more difficult to venture whether they would be enzymatically active if tested in vitro for aminoacylation and pyrophosphate exchange activity. In that regard, mutant 3 is the most promising. Its conformation is largely preserved in all three complexes tested, which amount to a total of 2000 ps of molecular dynamics. It presents two alternate structures in complex with His+ATP, depending on the 273–281 loop conformation; the lowest energy structure is very similar to the SerRS active site structure. This structure seems to have the attributes for carrying out the activation of histidine, although it may not perform as well as wild-type HisRS. To test these predictions, the mutants will be engineered and studied biochemically.

ACKNOWLEDGMENTS

We thank Prof. C. Francklyn for discussions and careful reading of the manuscript. Some of the simulations were performed at the Centre National Universitaire Sud de Calcul (Ministère de l'Education Nationale). The CHARMM program was kindly provided by Prof. M. Karplus.

REFERENCES

1. Eriani, G., Delarue, M., Poch, O., Gangloff, J. , Moras, D. Partition of tRNA synthetases into two classes based on mutually exclusive sets of sequence motifs. Nature 347:203–206, 1990.
2. Moras, D. Structural and functional relationships between aminoacyl-tRNA synthetases. Trends Biochem. Sci. 17:159–164, 1992.

3. Arnez, J.G. , Moras, D. Structural and functional considerations of the aminoacylation reaction. Trends Biochem. Sci. 22:211–216, 1997.
4. Arnez, J.G., Harris, D.C., Mitschler, A., Rees, B., Francklyn, C.S. , Moras, D. Crystal structure of histidyl-tRNA synthetase from *E. coli* complexed with histidyl-adenylate. EMBO J. 14:4143–4155, 1995.
5. Arnez, J.G., Augustine, J.G., Moras, D., Francklyn, C.S. The first step of aminoacylation at the atomic level in histidyl-tRNA synthetase. Proc. Natl. Acad. Sci. U.S.A. 94:7144–7149, 1997.
6. Belrhali, H., Yaremchuk, A., Tukalo, M., et al. The structural basis for seryl-adenylate and Ap_4A synthesis by seryl-tRNA synthetase. Structure 3:341–352, 1995.
7. Beese, L.S. , Steitz, T.A. Structural basis for the 3'-5' exonuclease activity of *Escherichia coli* DNA polymerase I: A two metal ion mechanism. EMBO J. 10:25–33, 1991.
8. Fothergill, M., Goodman, M.F., Petruska, J. , Warshel, A. Structure-energy analysis of the role of metal ions in phosphodiester bond hydrolysis by DNA polymerase I. J. Am. Chem. Soc. 117:11619–11627, 1995.
9. Cavarelli, J., Eriani, G., Rees, B., et al. The active site of yeast aspartyl-tRNA synthetase: Structural and functional aspects of the aminoacylation reaction. EMBO J. 13:327–337, 1994.
10. Poterszman, A., Delarue, M., Thierry, J.-C., Moras, D. Synthesis and recognition of aspartyl-adenylate by *Thermus thermophilus* aspartyl-tRNA synthetase. J. Mol. Biol. 244:158–167, 1994.
11. Kennard, O., Isaacs, N.W., Motherwell, W.D.S., et al. Crystal and molecular structure of adenosine triphosphate. Proc. R. Soc. Lond. A 325:401, 1971.
12. Sugawara, Y., Kamiya, N., Iwasaki, H., Ito, T., Satow, Y.J. Humidity-controlled reversible structure transition of disodium adenosine 5′-triphosphate between dihydrate and trihydrate in a single crystal state. Am. Chem. Soc. 113: 5440, 1991.
13. Sabat, M., Cini, R., Haromy, T., Sundaralingam, M. Crystal structure of the alpha, beta, gamma-tridentate manganese complex of adenosine 5'-triphosphate cocrystallized with 2,2'-dipyridylamine. Biochemistry 24:7827–7833, 1985.
14. Cini, R., Burla, M.C., Nunzi, A., Polidori, G.P., Zanazzi, P.F. Preparation and physico-chemical properties of the ternary complex formed between adenosine 5′-triphosphoric acid, bis(2-pyridyl)amine, and divalent metal ions. Crystal and molecular structures of the compounds containing Mg^{2+} and Ca^{2+}. J. Chem. Soc. Dalton Trans. 2467, 1984.
15. Roberts, V.A., Getzoff, E.D. Metalloantibody design. FASEB J. 9:94–100, 1995.
16. Regan, L. Protein design: Novel metal-binding sites. Trends Biochem. Sci. 20:280–285, 1996.
17. Hellinga, H. Metalloprotein design. Curr. Opin. Biotech. 7:437–441, 1996.
18. Lu, Y., Valentine, J.S. Engineering metal-binding sites in proteins. Curr. Opin. Struct. Biol. 7:495–500, 1997.
19. Yeung, B.K.S., Wang, X., Sigman, J.A., Petillo, P.A. , Lu, Y. Construction and characterization of a magnesium-binding site in cytochrome c peroxidase: Toward a novel manganese peroxidase. Chem. Biol. 4:215–222, 1997.
20. Durussel, I., Pauls, T.L., Cox, J.A., Berchtold, M.W. Chimeras of parvalbumin and oncomodulin involving exchange of the complete CD site show that the Ca^{2+}/Mg^{2+} specificity is an intrinsic property of the site. Eur. J. Biochem. 242:256–263, 1997.
21. Åberg, A., Yaremchuk, A., Tukalo, M., Rasmussen, B., Cusack, S. Crystal structure of the activation of histidine by *Thermus thermophilus* histidyl-tRNA synthetase. Biochemistry 36:3084–3094, 1997.
22. MacKerell, A.D., Bashford, D., Bellott, M., et al. An all-atom empirical potential for molecular modelling and dynamics study of proteins. J. Phys. Chem. B 102:3586–3616, 1998.
23. Jorgensen, W., Chandrasekar, J., Madura, J., Impey, R., Klein, M. Comparison of simple potential functions for simulating liquid water. J. Chem. Phys. 79:926–935, 1983.
24. Neria, E., Fischer, S. , Karplus, M. Simulation of activation free energies in molecular systems. J. Chem. Phys. 105: 1902–1921, 1996.
25. Simonson, T. Accurate calculation of the dielectric constant of water from simulations of a microscopic droplet in vacuum. Chem. Phys. Lett. 250:450–454, 1996.
26. Brooks III, C., Brünger, A.T. , Karplus, M. Active site dynamics in proteins: A stochastic boundary molecular dynamics approach. Biopolymers 24:843–865, 1985.
27. Simonson, T., Archontis, G. , Karplus, M. Continuum treatment of long-range interactions in free energy calculations. Application to protein-ligand binding. J. Phys. Chem. B. 101:8349–8362, 1997.
28. Ryckaert, J., Ciccotti, G. , Berendsen, H. Numerical integration of the cartesian equations of motion for a system with constraints: Molecular dynamics of n-alkanes. J. Comp. Phys. 23:327–341, 1977.
29. Press, W.H., Flannery, B.P., Teukolsky, S.A., Vetterling, W.T. "Numerical Recipes." Cambridge University Press, Cambridge, 1986.
30. Brünger, A.T. "X-PLOR Version 3.1. A System for X-ray Crystallography and NMR." New Haven, CT: Yale University Press, 1992.
31. Brooks, B., Bruccoleri, R., Olafson, B., States, D., Swaminathan, S., Karplus, M. CHARMM: A program for macromolecular energy minimization and molecular dynamics calculations. J. Comp. Chem. 4:187–217, 1983.
32. Stote, R., Karplus, M. Zinc binding in proteins and in solution: A simple but accurate nonbonded representation. Proteins 23:12–31, 1995.
33. Archontis, G., Simonson, T., Moras, D., Karplus, M. Specific amino acid recognition by aspartyl-tRNA synthetase studied by free energy simulations. J. Mol. Biol. 275:823–846.
34. Schmitt, E., Thierry, J.C., Moras, D. AspRS from Archae. in preparation, 1998.
35. MacKerell, A.D. Influence of magnesium ions on duplex DNA structural, dynamic, and solvation properties. J. Phys. Chem. B. 101:646–650, 1997.
36. Cowan, J.A. "The Biological Chemistry of Magnesium." VCH, New York, 1995.
37. Lybrand, T., Kollman, P. Water-water and ion-water potential functions including terms for many-body effects. J. Chem. Phys. 83:2923–2933, 1985.
38. Logan, D.T., Mazauric, M.H., Kern, D., Moras, D. Crystal structure of glycyl-tRNA synthetase from *Thermus thermophilus*: New functional domains and substrate specificity. EMBO J. 14:4156–4167, 1995.
39. Onesti, S., Miller, A.D., Brick, P. The crystal structure of the lysyl-tRNA synthetase (LysU) from *Escherichia coli*. Structure 3:163–176, 1995.
40. Mosyak, L., Reshetnikova, L., Goldgur, Y., Delarue, M. , Safro, M.G. Structure of phenylalanyl-tRNA synthetase from *Thermus thermophilus*. Nature Struct. Biol. 2:537–547, 1995.
41. MacKerell, A.D., Wiorkiewicz-Kuczera, J., Karplus, M. An all-atom empirical energy force-field for the study of nucleic acids. J. Am. Chem. Soc. 117:11946–11975, 1995.
42. Frisch, M.J., Trucks, G.W., Head-Gordon, M., et al. "Gaussian92, Revision A." Pittsburgh, PA: Gaussian, Inc., 1992.
43. Kraulis, P.J. MOLSCRIPT: A program to produce both detailed and schematic plots of protein structures. J. Appl. Crystallogr. 24:946–950, 1991.
44. Bacon, D.J. , Anderson, W.F. A fast algorithm for rendering space-filling molecule pictures. J. Mol. Graphics 6:219–220, 1988.
45. Merritt, E.A. , Murphy, M.E.P. Raster 3D: A program for photorealistic molecular graphics. Acta Crystallogr. D50: 869–873, 1994.

APPENDIX: AMINOACYL-ADENYLATE FORCE FIELD PARAMETERS

The central part of the aminoacyl-adenylate, linking the amino acid and AMP moieties, is not parameterized in the CHARMM22 force field. We determine here parameters that should be suitable not

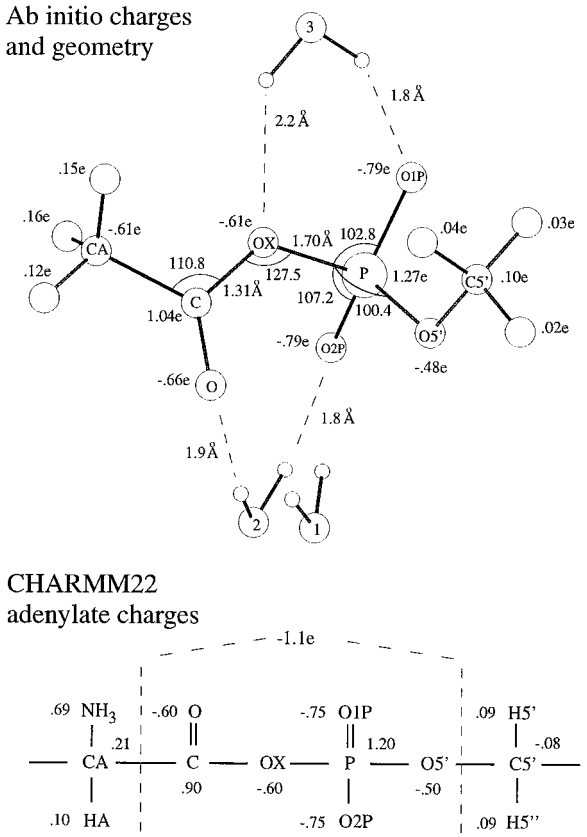

Fig. 11. **a:** Methylacetyl-phosphate. A water ligand is represented in three possible positions (see text). Ab initio bond lengths, angles, and atomic partial charges are indicated, as well as water-oxygen distances for positions 2 and 3. **b:** Partial charges for atoms in the region bridging the amino acid and AMP moieties of the aminoacyl-adenylate.

TABLE IV. Water-Methylacetylphosphate Interaction Energies (kcal/mol)

	CHARMM22‡			
Position†	Large OX	Small OX	MP2/ 6-311+G*§	HF/6-311 + G*§
1	−18.86	−18.83	−16.02	−12.67
2	−20.13	−20.11	−16.29	−13.30
3	−17.02	−17.24	−15.70	−12.62

†Water position in Figure 11.
‡Large (ϵ = 0.1521 kcal/mol, σ = 3.1539 Å) and small (ϵ = 0.1521 kcal/mol, σ = 2.7974 Å) CHARMM22 oxygen van der Waals parameters for OX.
§Basis set superposition error neglected.

only for histidyl-adenylate, but for all 20 aminoacyl adenylates. Consistent with the methods used to develop the CHARMM22 force field,[22,41] we consider a small molecule analogous to the central part of the adenylate, methylacetyl-phosphate (MAP; Fig. 11). We first determine initial charges and geometry from ab initio calculations at the 6–31G* level, and then we consider its interactions with a single water molecule; finally, the resulting parameters are transferred to the aminoacyl-adenylate and tested in molecular dynamics simulations (described above) of His-adenylate complexed to HisRS.

The geometry of MAP was optimized at the HF/6–31G* level using the program Gaussian92,[42] and

TABLE V. Aminoacyl-Adenylate Force Field Parameters: CHARMM22-Compatible Parameters for the Region of the Adenylate Linking the Amino Acid and the AMP

Atom	Atom type[a]	Charge[b]
N	NH3	−0.30
HT1	HC	0.33
HT2	HC	0.33
HT3	HC	0.33
CA	CT1	0.21
HA	HB	0.10
C	C	0.90
O	O	−0.60
OX	OX	−0.60
P	P	1.20
O1P	ON3	−0.75
O2P	ON3	−0.75
O5′	ON2	−0.50
C5′	CN8	−0.08
H5′	HN7	0.09
H5″	HN7	0.09

	Atom types			Force constant[c]	Target value[d]
Bond	C	OX		570	1.25
Bond	P	OX		270	1.60
Angle	CT1	C	OX	40	110.8
Angle	O	C	OX	100	126.7
Angle	C	OX	P	20	127.5
Angle	ON3	P	OX	100	105.0
Angle	ON2	P	OX	80	100.4

	Atom types				Force constant[e]	Periodicity[e]	Offset[e]
Dihe	CT2	CT1	C	OX	0.067	3	180.
Dihe	NH3	CT1	C	OX	0.067	3	180.
Dihe	X	OX	P	X	0.250	3	0.
Dihe	X	OX	C	X	0.000	3	0.
Dihe	CN8	ON2	P	OX	0.250	3	0.
Dihe	CN8	ON2	P	OX	0.750	2	0.
Dihe	HB	CT1	C	OX	0.000	1	0.

	Atom type	ϵ[f]	σ[g]	ϵ_{14}[h]	σ_{14}[h]
Nonbonded	OX	0.1521	3.1538	0.1521	3.1538

[a]CHARMM22 atom type.
[b]Fraction of electronic charge.
[c]kcal/mol/Å^2 (bonds) or kcal/mol/rad^2 (angles).
[d]Å (bonds) or degrees (angles).
[e]kcal/mol. The dihedral energy is given by $k(1 + \cos(n\phi + \delta))$, where k, n, and δ are the force constant, periodicity, and offset, respectively.
[f]kcal/mol.
[g]Å.
[h]Parameters for interactions between atoms separated by three covalent bonds.

atomic partial charges were obtained by fitting the ab initio electrostatic potential on a grid around the molecule. Results are shown in Figure 11.

The same procedure, when applied to dimethylphosphate, yields charges in good agreement with the CHARMM22 charges (results not shown). Stereochemical force constants and van der Waals parameters were taken from the CHARMM22 force field by considering the analogous amino acid backbone and AMP groups. For the bridging oxygen OX between the amino acid and AMP, two van der Waals assignments are possible: either the "large" or "small" CHARMM22 oxygen van der Waals parameters could be used, by analogy to O5' or O, respectively. Initially the "large" oxygen parameters were chosen. Thus parameterized, the fragment was immersed in a sphere of modified TIP3P water molecules (see Materials and Methods), the energy minimized, and all waters except the one closest to OX discarded. This water bridges O and O2P (position 1 in Fig. 11). After molecular mechanics minimization with the "large" OX, it shifts slightly closer to O (position 2 in Fig. 11). Minimizing from position 1 with a "small" OX (analogous to O, O1P, O2P), the water shifts to the other side of the phosphate (position 3). Minimizing from position 1 with HF/3–21G*, the water shifts to the right, away from OX, closer to the phosphate (not shown). The HF/6–311+G*, MP2/6–311+G*, and molecular mechanics energies of positions 1–3 are shown in Table IV. Basis set superposition error was neglected. Although the molecular mechanics energies only reproduce the ab initio energies approximately, they rank the three conformations in the correct order, and furthermore, they are very insensitive to the choice of OX van der Waals parameters. Clearly, the energy and position of a water close to OX are dominated by the nearby, negatively charged phosphate group, and the exact van der Waals parameters of OX are not critical. Thus, the present parameters (Table V), with the "large" OX, were transferred without further adjustment to the histidyl-adenylate and tested in molecular dynamics simulations of the HisRS:HisAMP complex. Good agreement was observed with the crystal structure for the region around the adenylate, as described in Results. The parameters for the bridging region should be suitable for all 20 aminoacyl-adenylates.